Self-Assembly of Metallo-Supramolecules under Kinetic or Thermodynamic Control? Characterization of Positional Isomers Using Scanning Tunneling Spectroscopy

Lei Wang,[†,▽] Bo Song,[†,▽] Yiming Li,[†,▽] Lele Gong,[⊥] Xin Jiang,[≛] Ming Wang,[≛] Shuai Lu,[†,∥] Xin-Qi Hao,[∥] Zhenhai Xia,[⊥] Yuan Zhang,*[,‡,§] Saw Wai Hla*[,‡] and Xiaopeng Li*[,†]

[†]Department of Chemistry, University of South Florida, Tampa, Florida 33620, United States
[⊥]Department of Materials Science and Engineering, University of North Texas, Denton, TX 76203, United States
[≛]State Key Laboratory of Supramolecular Structure and Materials, College of Chemistry, Jilin University, Changchun, Jilin 130012, China
[∥]College of Chemistry, Zhengzhou University, Zhengzhou, Henan 450052, China
[‡]Nanoscience and Technology Division, Argonne National Laboratory, Lemont, IL 60439, United States
[§]Department of Physics, Old Dominion University, Norfolk, Virginia 23529, United States

KEYWORDS: metallo-supramolecules, supramolecular isomerism , self-assembly, scanning tunneling microscopy, terpyridine

ABSTRACT: Coordination-driven self-assembly has been extensively employed to construct a variety of discrete structures as a bottom-up strategy. However, mechanistic understanding regarding whether self-assembly is under kinetic or thermodynamic control is less explored. To date, such mechanistic investigation has been limited to distinct, assembled structures. It still remains a formidable challenge to study the kinetic and thermodynamic behavior of self-assembly systems with multiple assembled isomers due to the lack of characterization methods. Herein, we use a stepwise strategy which combined a self-recognition and self-assembly process to construct giant metallo-supramolecules with 8 positional isomers in solution. With the help of ultrahigh-vacuum, low-temperature scanning tunneling microscopy and scanning tunneling spectroscopy, we were able to unambiguously differentiate 14 isomers on substrate which correspond to 8 isomers in solution. Through measurement of 162 structures, the experimental probability of each isomer was obtained and compared with the theoretical probability. Such a comparison along with density functional theory (DFT) calculation suggested that although both kinetic and thermodynamic control existed in this self-assembly. The increased experimental probabilities of isomers compared to theoretical probabilities should be attributed to thermodynamic control.

Introduction

Because of its intrinsic dynamic nature, self-assembly is able to organize suitable molecular components into more sophisticated supramolecular entities by virtue of non-covalent interactions.[1] Typically, self-assembly involves multiple reversible processes of dissociation, association, and reorganization in which the structures or properties can be tuned by physical conditions or external stimulus.[2] Studies have revealed that factors such as ligand geometry, metal ions/anions, reaction time, temperature, concentration, and solvent can affect the final products of self-assembly.[3] Beyond these factors, the assembled structures could also be determined by kinetic control or thermodynamic control.[2b] In the majority of systems, the reversible and weak, non-covalent interactions favor thermodynamically controlled structures with optimum conditions.[4] In contrast, kinetically controlled self-assembly can form inert structures using less labile interactions,[5] or metastable products that are kinetically trapped at local minima[6-7] and may be further transformed to more stable products upon prolonged reaction time.[7] In one of the pioneering works, Lehn and coworkers revealed that the triple helicate assembled by a tris-bipyridine ligand could progressively convert into the circulate helicate, corresponding to the switch from kinetic control to thermodynamic control.[7a] In Fujita's self-assembled M_nL_{2n} polyhedra, they were considered as thermodynamically controlled products when n = 6, 12, or 24. While for n > 24, the kinetic trapping is no longer negligible.[6c] As such, $M_{30}L_{60}$ and $M_{48}L_{49}$ assembled by the same ligand with Pd(II) were categorized as kinetically and thermodynamically controlled products, respectively.[7d] It is worth noting that these assemblies generally gave distinct assembled structures regarding kinetic or thermodynamic control, facilitating detailed characterization.

Supramolecular isomerism has been well studied in coordination polymers and metal-organic frameworks which highly rely on crystal engineering to confirm the structure explicitly.[8] In coordination-driven self-assembly of discrete metallo-supramolecules, more attention was focused on precise control over the shape and size of assemblies.[9]

Through careful design, a single metallo-supramolecule rather than a mixture of isomers

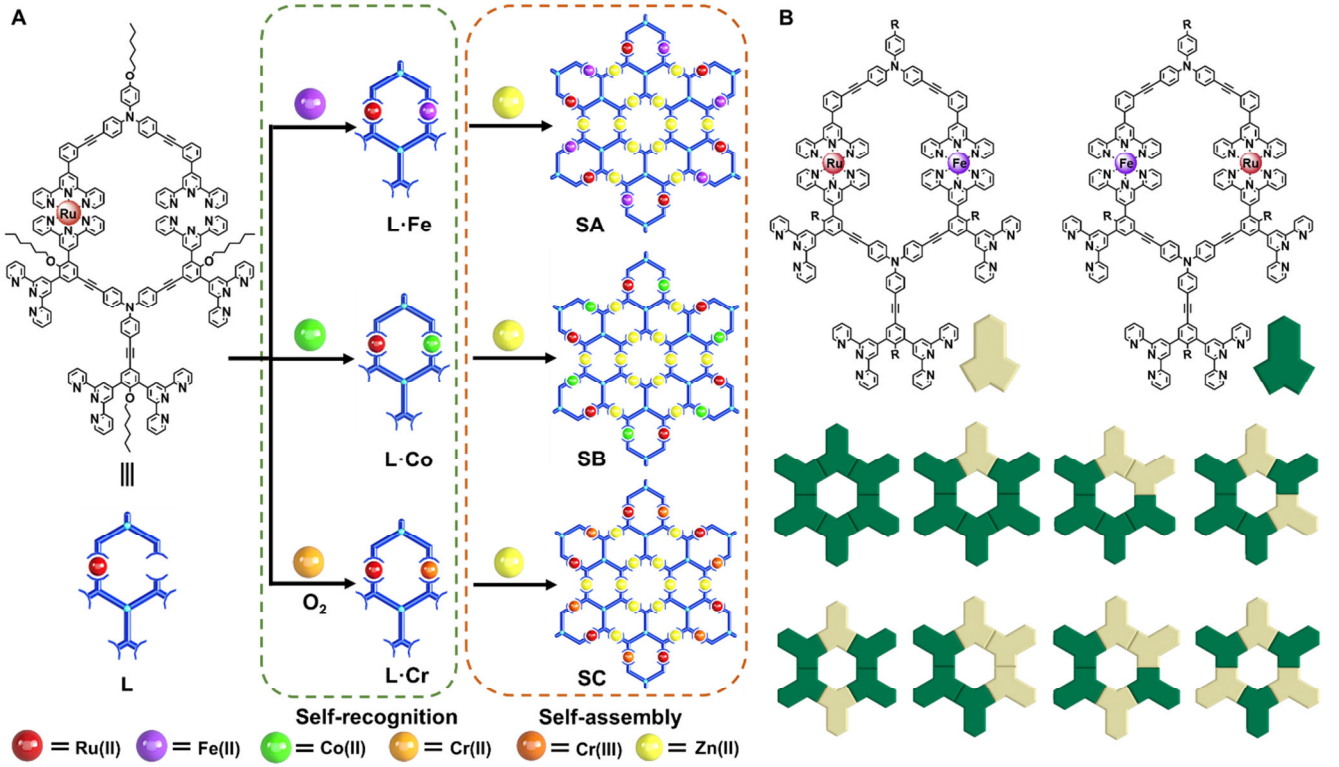

Figure 1. (A) Construction of three trimetallic supramolecules **SA**-**SC** through self-recognition and self-assembly; (B) Eight isomers generated in solution after self-assembly.

were obtained in individual self-assembly.[10] However, isomerism sometimes still occurred, for instance, positional isomers from the unbiased arrangement of dissymmetrical building blocks,[11] configurational isomers from the asymmetric chelating ligand arrangements around the metal centers,[12] social and constellation isomers through different arrangement/orientation of guests encapsulated in a confined host,[13] and unidentical packing modes during crystallization process.[14] Such supramolecular isomerization at the molecular level is expected to increase the complexity and diversity of supramolecular chemistry, and thus has resulted in applications in molecular devices and optics.[15] However, supramolecular isomerism in discrete metallo-supramolecules remains less explored compared to MOFs and polymers, perhaps due to the lack of platforms with rational, precise design and insufficient characterization by NMR,[13,15] crystal engineering,[12,14] ion mobility-mass spectrometry (IM-MS)[10a] and molecular modeling.[11a,16]

In the present work, we demonstrated the construction of three giant trimetallic supramolecules through the self-recognition and self-assembly of a metal-organic ligand **L**. As a consequence of intramolecular and intermolecular complexation, three types of metal ions were successfully incorporated into the discrete metallo-supramolecules using terpyridine (tpy)-based[17] coordination chemistry to form <tpy-M-tpy> connectivities in a stepwise manner (Figure 1A). Because of the dissymmetrical nature of the intermediate **L·M** after self-recognition, eight positional isomers were formed in the self-assembly of the final supramolecules in solution (Figure 1B). In terms of large molecular weight and high complexity, it remains a formidable challenge to address whether the self-assembly of those positional isomers is under kinetic and/or thermodynamic control with conventional characterization methods. Herein we report the combined use of ultrahigh-vacuum, low-temperature scanning tunneling microscopy (UHV-LT-STM)[18] and scanning tunneling spectroscopy (STS)[19] to characterize the isomers at the atomic level in this complex supramolecular system. Using these methods, we investigated the contribution of thermodynamic and kinetic control in the outcome of isomer distribution.

Results and Discussion

Synthesis of Trimetallic Supramolecules. The metal-organic tpy ligand **L** was synthesized with <tpy-Ru(II)-tpy> connectivity using a Ru(II) end-capping approach by performing a Sonogashira coupling reaction on the Ru-tpy complex (Scheme S1).[20] **L** possesses six free tpy for self-recognition and self-assembly. In the introduction of the second type of metal ion, one equivalent of either Fe(II), Co(II) or Cr(II) was mixed with **L** at 80 °C to form an exclusive intermediate (**L·M**) through specific coordination or self-recognition. Conventional electrospray ionization-mass spectrometry (ESI-MS) first suggested the formation of the proposed intermediates. The measured *m/z* agreed well with the molecular compositions of the intermediates, i.e., 849.81 for **L·Fe**, 850.56 for **L·Co** and 853.06 for **L·Cr** at charge state 4+ (Figures S35-S36), respectively. Here, Cr(II) was oxidized to Cr(III) by air bubbling and an -OH group is attached to balance the increased valence.[21] ^{1}H NMR was also applied to confirm the specific coordination

site within the structure of the intermediate **L·Fe**. Two sets of signals with metal and three sets of free tpy signals were observed in **L**; while four sets of coordinated tpy signals and three sets of free tpy signals were assigned in **L·Fe** because of the loss of molecular symmetry after complexation with an additional equivalent of Fe(II). The downfield shift of the tpy-E3′5′ signal and tpy-F3′5′ signal proved that Fe(II) was selectively coordinated through

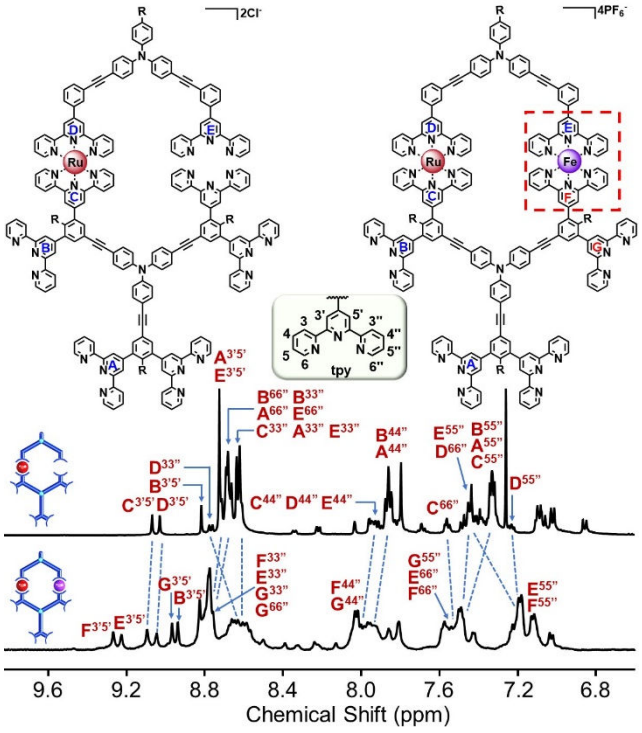

Figure 2. ^{1}H NMR spectra (500 MHz, 300 K) of **L** in $CDCl_3$ and **L·Fe** in CD_3CN.

self-recognition (Figure 2). Detailed assignments here were based on 2D COSY and 2D NOESY spectra (Figures S19–S22). However, the ^{1}H NMR spectra of **L·Co** and **L·Cr** are broad (Figures S24–S25) and unsatisfactory results were obtained for 2D NMR experiments because of the paramagnetic natures of Co(II) and Cr(III). Nevertheless, two sets of characteristic tpy signals spread out in a wide range (20 ~ 100 ppm) corresponding to the <tpy-Co(II)-tpy> connectivity[22] were identified in the proton NMR, supporting the formation of the proposed intermediate **L·Co** (Figure S24). We speculate that the exclusive formation of the intermediate is energetically more favorable through intramolecular complexation rather than intermolecular complexation.[23] Additionally, those metastable intermediates are reminiscent of folding in protein structures, resulting from conformational regulation.[24] Without further purification or separation, two equivalents of Zn(II) as the third type of metal ion were added to the reaction mixture for self-assembly for 8 h at 50 °C. Among these metal ions, Zn(II) has the weakest coordination with tpy to facilitate self-assembly without disturbing the previous metal ion coordination.[25c] After counterion exchange and washing, three targeted metallo-supramolecules with fractal pattern[25,20b] were obtained in high yield.

Characterization of Supramolecules. ESI-MS and traveling wave ion mobility-mass spectrometry (TWIM-MS)[26] are applied to provide structural information of the final heterometallic supramolecules. Only one set of continuous charged signals was observed from 1D ESI-MS (Figure 3A,3C; Figure S39a) corresponding to molecular weights of 28136, 28155, and 28215 Da for **SA**, **SB** and **SC**, respectively. A narrow distribution of drift time for each charge state in the TWIM-MS spectra (Figure 3B, 3D; Figure S39b) suggested a clean formation of discrete metallo-supramolecules with high shape-persistence.

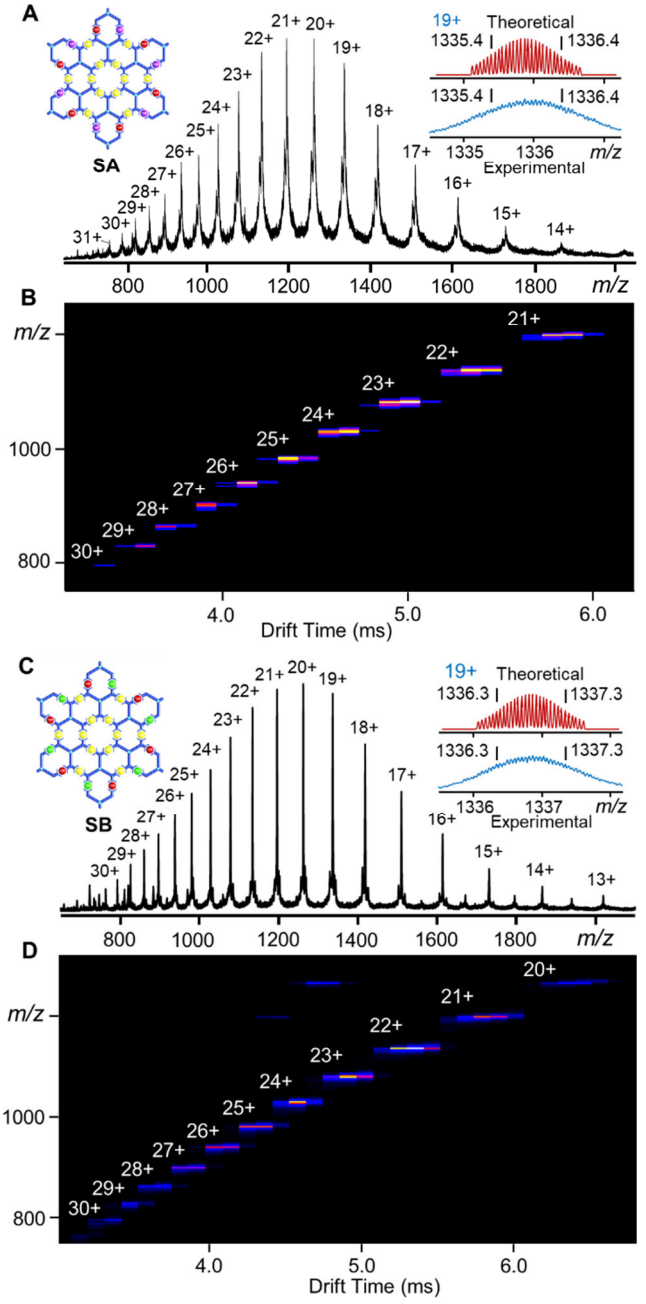

Figure 3. ESI-MS spectra of (A) **SA** and (C) **SB**; TWIM-MS plot (*m/z* vs. drift time) of (B) **SA** and (D) **SB**.

Furthermore, the corresponding isotope pattern measured for each charge state of the supramolecules agreed well with the theoretical one (i.e., 1335.9 for **SA**, 1336.8 for **SB**, 1340.0 for **SC** at charge state 19+), which strongly supports the formation of the proposed structure (Figures S40–S42). The mass spectrometry data excludes the possi-

bility of disassembly and reassembly of <tpy-Fe(II)-tpy>, <tpy-Co(II)-tpy> or <tpy-Cr(III)-tpy> within the targeted metallo-supramolecules. If disassembly and reassembly occurred, it is expected to observe multiple sets of signals in mass spectrometry corresponding to different numbers (0-18) of Fe(II), Co(II) or Cr(III) in the final assembled structure. Gradient tandem-mass spectrometry (gMS^2)[27]

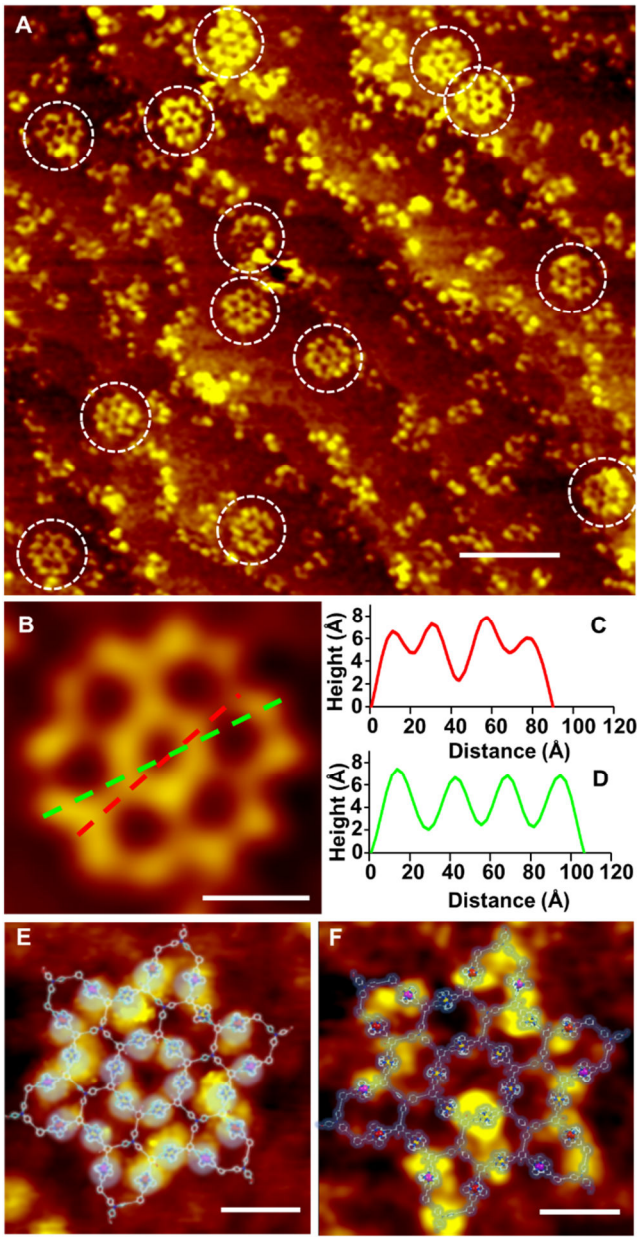

Figure 4. (A) Large area STM image with supramolecule **SA** randomly anchored (scale bar 10 nm, scanning parameters: V_t = 2V, I_t = 130pA); (B) Zoomed-in STM image for line profile measurements(scale bar 2 nm, scanning parameters: V_t = 2V, I_t = 130pA); (C and D) The STM line profile measurements along green and red dashed lines inside the hexagon grid shown in (B); Topography of **SA** at (E) bias voltage = +2V (scale bar 2 nm, scanning parameters V_t = 2V, I_t = 50pA) and (F) bias voltage = -2V (scale bar 2 nm, scanning parameters V_t = -2V, I_t = 50pA) with molecular modelling overlay.

showed that the three supramolecules were all fully dissociated at +25 V, corresponding to a center-of-mass collision energy of 0.04 eV. This implies similar stability of these three metallo-supramolecules in the gas phase despite three different metal ions are incorporated (Figures S43–S45). Thus, the stability of the whole supramolecule is determined by the weakest <tpy-Zn(II)-tpy> among the three <tpy-M-tpy> connectivity.[28]

Due to each **L·M** having two different orientations in the self-assembly with Zn(II), the final metallo-supramolecules would generate eight isomers (Figures S47–S48) leading to very broad NMR spectra. Nevertheless, the characteristic signals in ^{1}H NMR, 2D COSY and 2D NOESY spectra of complex **SA** were still assigned consistent with the proposed structure (Figures S28–S32). Diffusion-ordered NMR spectroscopy (DOSY) showed the diffusion coefficient (D, m^2/s) of **SA** to be 1.43 $\times 10^{-10}$, which corresponded to an experimental hydrodynamic radius (r_H) of 5.7 nm.[17e,20] This also agreed with the molecular diameter obtained from modeling (r = 5.5 nm) (Figure S34).

In addition to the structural characterization described above, UHV-LT-STM was utilized to directly visualize the structures of the giant metallo-supramolecules. Working by the mechanism of quantum tunneling effects under a small bias voltage ±1-2 V, STM effectively prevents molecular structural damages such as knock-on damages, heating effects, and radiolysis that can be introduced by other microscopy characterization methods.[29] Moreover, STM investigations can provide detailed information on topography and electronic properties at the atomic scale, making it more powerful for the characterization of self-assembled structures.[30] Since all three types of supramolecules are nearly identical in shape, **SA** was selected as a representative for STM characterization. For the STM experiments, a freshly prepared sample solution of **SA** (1×10^{-5} M) in acetonitrile was dropped on a Ag (111) surface and then the sample was cooled down to ~5 K to reduce thermal motion of the molecules thereby a high resolution was achieved. Remarkably, intact supramolecules were observed directly in the scanned areas with some fragments absorbed on the surface (Figures 4A, S46). Note that the supramolecules can undergo disassembly via the weakest <tpy-Zn(II)-tpy> in a very dilute solution. With an applied positive voltage of +2 V, each <tpy-M-tpy> connection unit was visualized as a bright lobe in the STM image while the overall organic backbone of the supramolecule was well displayed at the negative bias voltage of -2 V (Figure 4E and 4F). The measured height (*ca.* 6 Å) and as well as the diameter (*ca.* 1.1 and 1.0 nm) perfectly matched the size and dimension predicted by theoretical modeling (Figures 4B, 4C, 4D).

Identification of Isomers. With a well visualized molecular structure by STM imaging, another important question regarding the existence of isomers still remains. As mentioned earlier, the intermediate **L·M** is dissymmetrical in chemical composition and it can flip over during the self-assembly with Zn(II), leading to the formation of 8 positional isomers with different orientations of Ru vs Fe in solution (Figures S47, S48). The identification of those positional isomers is extremely challenging using conventional characterization methods, e.g., mass spectrometry, NMR and X-ray diffraction. Therefore, scanning tunneling spectroscopy (STS) was employed here to probe the local

density of states (LDOS) for each metal junction to differentiate these isomers at the atomic scale.[19] Notably, 14 positional isomers are expected on the substrate (Figure 5A)

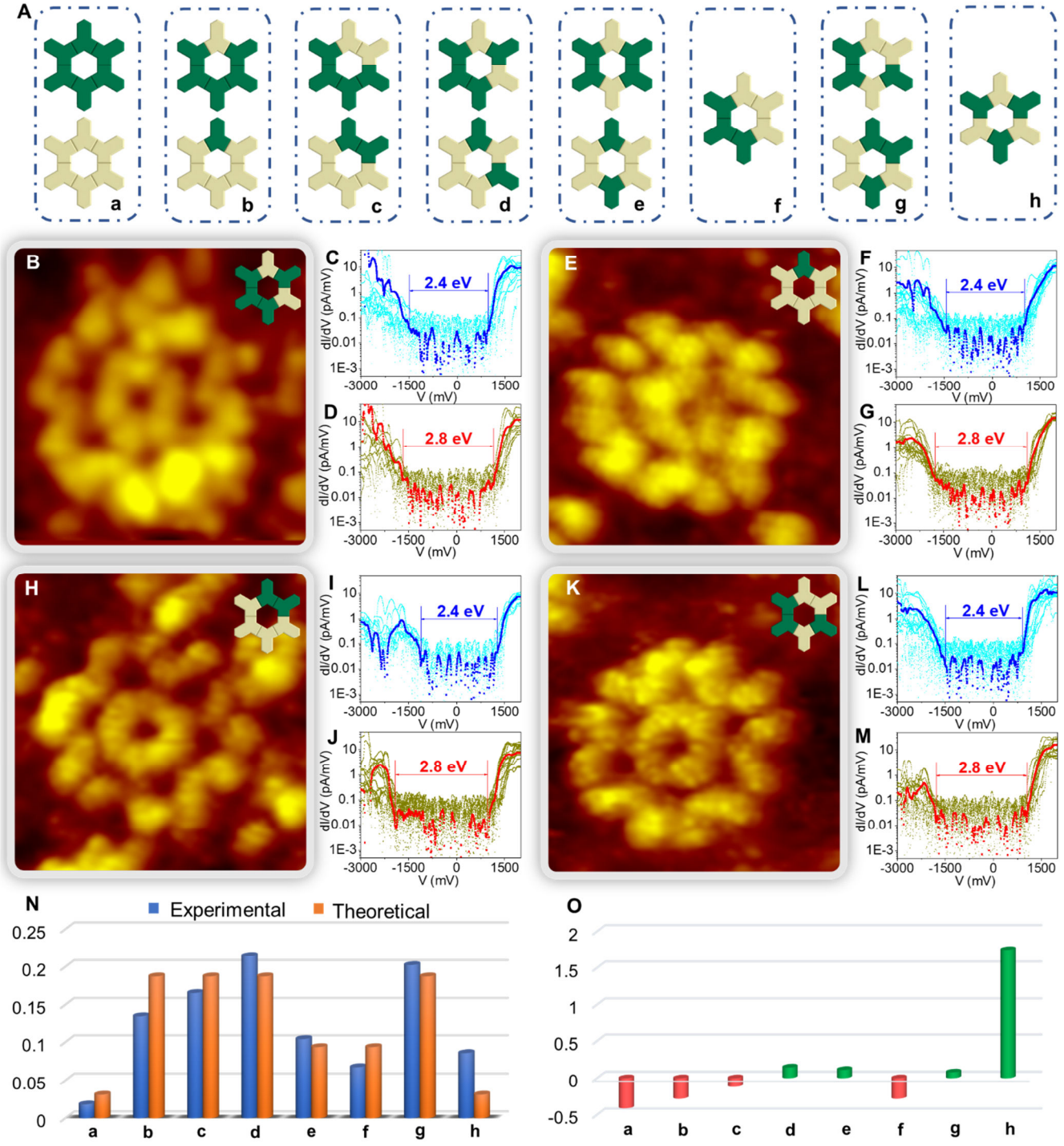

Figure 5. (A) 14 isomers generated on substrate, and the corresponding 8 isomers in solution, which were labelled **a**-**h**, respectively; (B, E, H, K) STM images of four isomers of **SA** determined by STS (scanning parameters: V_t = 2.5V, I_t = 48pA); (C, F, I, L) dI/dV-V tunneling spectroscopy data of Fe(II) (blue) corresponding to the supramolecules shown in B, E, H, K; (D, G, J, M) dI/dV-V tunneling spectroscopy data of Ru(II) (red) corresponding to the supramolecules shown in B, E, H, K; (N) Histogram of experimental and theoretical probability (P_E & P_T) for eight isomers in solution after measuring 162 supramolecules; (O) Histogram of relative deviation δ of eight isomers in solution calculated from experimental and theoretical probabilities ($\delta = [(P_E - P_T)/P_T]$).

because the two sides of each single molecule are no longer identical when depositing sample solution on the surface of Ag (111) for STS measurement. In order to avoid confusion, those two isomers with relative same positions of Ru vs Fe while two sides of molecules are considered the same type of isomers when doing the statistic calculation discussed below. Additionally, the probability of those two isomers regarding the different sides of same type of supramolecule were found equally on the substrate (Figure

S61), further supporting our classification for isomer types as reasonable.

Table 1. The Total Energy (eV) of Eight Isomers Calculated from DFT

Isomer	**a**	**b**	**c**	**d**	**e**	**f**	**g**	**h**
Energy	−12.36	−13.17	−13.03	−16.87	−16.06	−12.71	−18.13	−18.28

We first measured the LDOS of the metal junctions of a reference molecule **G5**[20b], which contains only one type of metal ion Ru(II) in its outermost ring. The obtained STS data in a single molecule showed a distinct average bandgap of 2.8 eV (Figure S49), which later serves as the reference to identify <tpy-Ru(II)–tpy>. As a following step, the STS data was collected for all the twelve metal junctions in the outermost ring of a single **SA** supramolecule. After careful analysis of the data and classifying the values into two groups, an average of 2.8 eV bandgap was observed for six metal junctions which could be assigned to <tpy-Ru(II)–tpy> according to the reference. Meanwhile, an averaged bandgap of 2.4 eV was found for the other six lobes, corresponding to <tpy-Fe(II)-tpy> (Figure 4B–4M). As such, we are able to differentiate each Fe(II) from Ru(II) based on the bandgap in a single molecule and successively determine the type of isomers out of the fourteen possible on the substrate (Figures 5B, 5E, 5H, 5K).

Such STS measurements were extended to a total of 162 supramolecules (Figures S50–S57), which allowed us to characterize all the 14 isomers on the Ag (111) surface (Figures 4B–4M, S58) for distribution analysis. Subsequent statistical study was performed to investigate the experimental and theoretical probability distributions. Overall, the experimental probabilities (P_E) basically followed the trend of the theoretical probabilities (P_T) (examined by chi-square test for independence, Table S1-S3) but displayed variations from isomers (Figure 5N). It should be noted that P_T is calculated mathematically (Figure S59) and is primarily viewed as the result of self-assembly under kinetical control. To better present the variations between P_E and P_T , we calculated the relative deviation δ using the formula $\delta = [(P_E - P_T)/P_T]$ (Figure S60) and the results were plotted in histogram as shown in Figure 5O. Isomers **a** and **h** have the same P_T of 0.0313, but experimental result showed an opposite trend which lead to a negative δ value of -0.41 for isomer **a**, while highest δ value of +1.77 for isomer **h**. Meanwhile, isomers **b**, **c**, and **f** all showed negative δ values and isomers **d**, **e**, and **g** showed positive δ values. These results implied that the second intramolecular complexation might not be dominated by kinetic control only, thermodynamic control also played an important role which lead to an energy-biased isomer distribution.

Considering that the difference only comes from the relative position of Ru vs Fe in the outermost ring in the chemical structure of isomers, **a**-**h**, we proposed that the system could be energy-favored when the same kinds of metals on the outer layer were neighboring on adjacent ligands to reduce electrostatic interactions between different metals. In other words, the total energy of the eight isomers should follow such a trend: **a**>**b**, **c**, **f**>**d**, **e**, **g**>**h** based on the increasing number of same neighboring metal ions on adjacent ligands (Figure S48). Our hypothesis was further supported by theoretical calculations, in which, density functional theory (DFT) was applied to calculate the total energy of each isomer by using the Vienna Ab initio Simulation Package (VASP) code with the Hubbard U (DFT+U) corrections.[31] Note that only metal ions in the isomers were extracted to simplify the calculation (Figure S1). As shown in Table 1, isomer **a** has the highest total energy of –12.36 eV compared to the lowest one of –18.28 eV for isomer **h,** which is suggested as the thermodynamically controlled product among 8 isomers. And the energy levels of other isomers are also in agreement with our proposed trend. At this point, we can conclude that the generation of these positional isomers was determined by kinetic and thermodynamic controls simultaneously; while thermodynamic control might play a more predominant role for the isomers with higher probabilities than theoretical ones. We speculated that the ligands could initially self-assemble with Zn(II) to form the kinetically stable isomers based on mathematical statistics, then thermodynamic control enabled the self-assembly to rearrange the distribution and enhanced the formation of the more energy-favored structures.[32]

Conclusions

In conclusion, we have successfully constructed a series of trimetallic supramolecules in one pot using the strategy of self-recognition and self-assembly. Through self-recognition, Fe(II), Co(II) or Cr(III) selectively coordinated with the pre-organized metal-organic ligand to form exclusive intermediates that were kinetically trapped. The subsequent self-assembly with the weakly coordinating metal ion Zn(II) afforded the final supramolecules **SA**-**SC** with more diversity through the formation of 8 positional isomers. The intermediates and the supramolecules were well characterized by mass spectrometry and NMR spectroscopy. **SA** was directly visualized using UHV-LT-STM and all the 8 isomers in solution (corresponding to 14 isomers on substrate) were successfully identified using STS to probe the local chemical environment with the LDOS at the atomic level. More importantly, the occurrence of supramolecular isomerism in our system was found to be determined by thermodynamic and kinetic control collaboratively using statistical study and DFT calculation. And their contributions were quantitatively understood through the deviation between the theoretical probability and experimental probability measured from the STS method we developed. Therefore, this study demonstrates that we are able to study the kinetic and thermodynamic features of supramolecular isomerism at single molecular level in a complicated system. Additionally, those trimetallic metallo-supramolecules may introduce metal-dependent proper-

ties and offer potential opportunities for future applications.

ASSOCIATED CONTENT

Supporting Information

Synthetic details, ligands and complexes characterization including ^{1}H NMR, ^{13}C NMR, 2D COSY, 2D NOESY, ESI-MS, TWIM-MS, STM and STS spectra are included in supporting information. The Supporting Information is available free of charge on the ACS Publications website.

AUTHOR INFORMATION

Corresponding Author

xiaopengli1@usf.edu
shla@anl.gov
y7zhang@odu.edu

Author Contributions

∇ L.W. ,B.S. and Y.L. contributed equally.

ORCID

Lei Wang: 0000-0002-3778-2814
Bo Song: 0000-0002-4337-848X
Yiming Li: 0000-0003-4602-3905
Xin Jiang: 0000-0003-2143-3596
Ming Wang: 0000-0002-5332-0804
Xin-Qi Hao: 0000-0003-1942-8309
Saw Wai Hla: 0000 0002 6463 9714
Xiaopeng Li: 0000-0001-9655-9551

Notes

The authors declare no competing financial interests.

ACKNOWLEDGMENT

This research was supported by National Institutes of Health (R01GM128037). Use of the Center for Nanoscale Materials, an Office of Science user facility, was supported by the U.S. Department of Energy, Office of Science, Office of Basic Energy Sciences, under Contract No. DE-AC02-06CH11357.

REFERENCES

(1). (a) Philp, D.; Stoddart, J. F. Self-Assembly in Organic Synthesis. *Synlett* **1991**, *1991*, 445-458. (b) Davis, A. V.; Yeh, R. M.; Raymond, K. N. Supramolecular Assembly Dynamics. *Proc. Natl. Acad. Sci. U. S. A.* **2002**, 99, 4793–4796. (c) Lehn, J.-M. From Supramolecular Chemistry Towards Constitutional Dynamic Chemistry and Adaptive Chemistry. *Chem. Soc. Rev.* **2007**, *36*, 151–160.

(2) (a) McConnell, A. J.; Wood, C. S.; Neelakandan, P. P.; Nitschke, J. R. Stimuli-Responsive Metal–Ligand Assemblies. *Chem. Rev.* **2015**, *115*, 7729-7793. (b) Liu, L.; Lyu, G.; Liu, C.; Jiang, F.; Yuan, D.; Sun, Q.; Zhou, K.; Chen, Q.; Hong, M. Controllable Reassembly of a Dynamic Metallocage: From Thermodynamic Control to Kinetic Control. *Chem. Eur. J.* **2017**, *23*, 456-461.

(3) (a) Hasenknopf, B.; Lehn, J.-M.; Boumediene, N.; Dupont-Gervais, A.; Van Dorsselaer, A.; Kneisel, B.; Fenske, D. Self-Assembly of Tetra- and Hexanuclear Circular Helicates. *J. Am. Chem. Soc.* **1997**, *119*, 10956-10962. (b) Stephenson, A.; Argent, S. P.; Riis-Johannessen, T.; Tidmarsh, I. S.; Ward, M. D. Structures and Dynamic Behavior of Large Polyhedral Coordination Cages: An Unusual Cage-to-Cage Interconversion. *J. Am. Chem. Soc.* **2011**, *133*, 858-870. (c) Bolliger, J. L.; Ronson, T. K.; Ogawa, M.; Nitschke, J. R. Solvent Effects Upon Guest Binding and Dynamics of a $Fe^{II}_4L_4$ Cage. *J. Am. Chem. Soc.* **2014**, *136*, 14545-14553. (d) Xie, T.-Z.; Endres, K. J.; Guo, Z.; Ludlow, J. M.; Moorefield, C. N.; Saunders, M. J.; Wesdemiotis, C.; Newkome, G. R. Controlled Interconversion of Superposed-Bistriangle, Octahedron, and Cuboctahedron Cages Constructed Using a Single, Terpyridinyl-Based Polyligand and Zn2+. *J. Am. Chem. Soc.* **2016**, *138*, 12344-12347. (e) Zhang, T.; Zhou, L.-P.; Guo, X.-Q.; Cai, L.-X.; Sun, Q.-F. Adaptive Self-Assembly and Induced-Fit Transformations of Anion-Binding Metal-Organic Macrocycles. *Nat. Commun.* **2017**, *8*, 15898-15906. (f) Wang, L.; Zhang, Z.; Jiang, X.; Irvin, J. A.; Liu, C.; Wang, M.; Li, X. Self-Assembly of Tetrameric and Hexameric Terpyridine-Based Macrocycles Using Cd(II), Zn(II), and Fe(II). *Inorg. Chem*. **2018**, *57*, 3548-3558.

(4) (a) Hasenknopf, B.; Lehn, J.-M.; Kneisel, B. O.; Baum, G.; Fenske, D. Self-Assembly of a Circular Double Helicate. *Angew. Chem. Int. Ed. Engl.* **1996**, *35*, 1838-1840. (b) Leininger, S.; Fan, J.; Schmitz, M.; Stang, P. J. Archimedean Solids: Transition Metal Mediated Rational Self-Assembly of Supramolecular-Truncated Tetrahedra. *Proc. Natl. Acad. Sci. U.S.A.* **2000**, *97*, 1380-1384. (c) Sun, Q.-F.; Iwasa, J.; Ogawa, D.; Ishido, Y.; Sato, S.; Ozeki, T.; Sei, Y.; Yamaguchi, K.; Fujita, M. Self-Assembled $M_{24}L_{48}$ Polyhedra and Their Sharp Structural Switch Upon Subtle Ligand Variation. *Science* **2010**, *328*, 1144-1147.

(5) (a) Ibukuro, F.; Kusukawa, T.; Fujita, M. A Thermally Switchable Molecular Lock. Guest-Templated Synthesis of a Kinetically Stable Nanosized Cage. *J. Am. Chem. Soc.* **1998**, *120*, 8561-8562. (b) Chepelin, O.; Ujma, J.; Barran, P. E.; Lusby, P. J. Sequential, Kinetically Controlled Synthesis of Multicomponent Stereoisomeric Assemblies. *Angew. Chem. Int. Ed.* **2012**, *51*, 4194-4197. (c) Xie, T.-Z.; Liao, S.-Y.; Guo, K.; Lu, X.; Dong, X.; Huang, M.; Moorefield, C. N.; Cheng, S. Z. D.; Liu, X.; Wesdemiotis, C.; Newkome, G. R. Construction of a Highly Symmetric Nanosphere Via a One-Pot Reaction of a Tristerpyridine Ligand with Ru(II). *J. Am. Chem. Soc.* **2014**, *136*, 8165-8168.

(6) (a) Paraschiv, V.; Crego-Calama, M.; Ishi-i, T.; Padberg, C. J.; Timmerman, P.; Reinhoudt, D. N. Molecular "Chaperones" Guide the Spontaneous Formation of a 15-Component Hydrogen-Bonded Assembly. *J. Am. Chem. Soc.* **2002**, *124*, 7638-7639. (b) Tashiro, S.; Tominaga, M.; Kusukawa, T.; Kawano, M.; Sakamoto, S.; Yamaguchi, K.; Fujita, M. Pd^{II}-Directed Dynamic Assembly of a Dodecapyridine Ligand into End-Capped and Open Tubes: The Importance of Kinetic Control in Self-Assembly. *Angew. Chem. Int. Ed.* **2003**, *42*, 3267-3270. (c) Fujita, D.; Ueda, Y.; Sato, S.; Yokoyama, H.; Mizuno, N.; Kumasaka, T.; Fujita, M. Self-Assembly of M30L60 Icosidodecahedron. *Chem.* **2016**, *1*, 91-101.

(7) (a) Hasenknopf, B.; Lehn, J.-M.; Boumediene, N.; Leize, E.; Van Dorsselaer, A. Kinetic and Thermodynamic Control in Self-Assembly: Sequential Formation of Linear and Circular Helicates. *Angew. Chem. Int. Ed.* **1998**, *37*, 3265-3268. (b) Hori, A.; Yamashita, K.-I.; Fujita, M. Kinetic Self-Assembly: Selective Cross-Catenation of Two Sterically Differentiated Pd^{II}-Coordination Rings. *Angew. Chem. Int. Ed.* **2004**, *43*, 5016-5019. (c) Yamanaka, M.; Yamada, Y.; Sei, Y.; Yamaguchi, K.; Kobayashi, K. Selective Formation of a Self-Assembling Homo or Hetero Cavitand Cage Via Metal Coordination Based on Thermodynamic or Kinetic Control. *J. Am. Chem. Soc.* **2006**, *128*, 1531-1539. (d) Fujita, D.; Ueda, Y.; Sato, S.; Mizuno, N.; Kumasaka, T.; Fujita, M. Self-Assembly of Tetravalent Goldberg Polyhedra from 144 Small Components. *Nature* **2016**, *540*, 563-566.

(8) (a) Moulton, B.; Zaworotko, M. J. From Molecules to Crystal Engineering: Supramolecular Isomerism and Polymorphism in Network Solids. *Chem. Rev.* **2001**, *101*, 1629-1658. (b) Zhang, J.-P.; Huang, X.-C.; Chen, X.-M. Supramolecular Isomerism in Coordination Polymers. *Chem. Soc. Rev.* **2009**, *38*, 2385-2396. (c) Karmakar, A.; Paul, A.; Pombeiro, A. J. L. Recent Advances on Supramolecular Isomerism in Metal Organic Frameworks. *CrystEngComm* **2017**, *19*, 4666-4695.

(9) (a) Chakrabarty, R.; Mukherjee, P. S.; Stang, P. J. Supramolecular Coordination: Self-Assembly of Finite Two- and Three-Dimensional Ensembles. *Chem. Rev.* **2011**, *111*, 6810-6918. (b)

Liu, Y.; Hu, C.; Comotti, A.; Ward, M. D. Supramolecular Archimedean Cages Assembled with 72 Hydrogen Bonds. *Science* **2011**, *333*, 436-440. (c) Ayme, J.-F.; Beves, J. E.; Campbell, C. J.; Leigh, D. A. Template Synthesis of Molecular Knots. *Chem. Soc. Rev.* **2013**, *42*, 1700-1712.

(10) (a) Schultz, A.; Li, X.; Barkakaty, B.; Moorefield, C. N.; Wesdemiotis, C.; Newkome, G. R. Stoichiometric Self-Assembly of Isomeric, Shape-Persistent, Supramacromolecular Bowtie and Butterfly Structures. *J. Am. Chem. Soc.* **2012**, *134*, 7672-7675. (b) Yu, H.-J.; Liu, Z.-M.; Yin, S.-Y.; Wu, K.; Wei, Z.-W.; Pan, M. Cage-Opening Supramolecular Isomerism in Cu(II) Complexes. *Inorg. Chem. Commun.* **2017**, *86*, 223-226. (c) Samantray, S.; Bandi, S.; Chand, D. K. Design of a Double-Decker Coordination Cage Revisited to Make New Cages and Exemplify Ligand Isomerism. *Beilstein J. Org. Chem.* **2019**, *15*, 1129-1140.

(11) (a) Zhao, L.; Northrop, B. H.; Zheng, Y.-R.; Yang, H.-B.; Lee, H. J.; Lee, Y. M.; Park, J. Y.; Chi, K.-W.; Stang, P. J. Self-Selection in the Self-Assembly of Isomeric Supramolecular Squares from Unsymmetrical Bis(4-Pyridyl)Acetylene Ligands. *J. Org. Chem.* **2008**, *73*, 6580-6586. (b) Song, B.; Kandapal, S.; Gu, J.; Zhang, K.; Reese, A.; Ying, Y.; Wang, L.; Wang, H.; Li, Y.; Wang, M.; Lu, S.; Hao, X.-Q.; Li, X.; Xu, B.; Li, X. Self-Assembly of Polycyclic Supramolecules Using Linear Metal-Organic Ligands. *Nat. Commun.* **2018**, *9*, 4575. (c) Lewis, J. E. M.; Tarzia, A.; White, A. J. P.; Jelfs, K. E. Conformational Control of Pd2L4 Assemblies with Unsymmetrical Ligands. *Chem. Sci.* **2020**, *11*, 677-683.

(12) (a) Wu, H.-B.; Wang, Q.-M. Construction of Heterometallic Cages with Tripodal Metalloligands. *Angew. Chem. Int. Ed.* **2009**, *48*, 7343-7345. (b) Meng, W.; Breiner, B.; Rissanen, K.; Thoburn, J. D.; Clegg, J. K.; Nitschke, J. R. A Self-Assembled M8L6 Cubic Cage That Selectively Encapsulates Large Aromatic Guests. *Angew. Chem. Int. Ed.* **2011**, *50*, 3479-3483. (c) Zhou, X.-P.; Liu, J.; Zhan, S.-Z.; Yang, J.-R.; Li, D.; Ng, K.-M.; Sun, R. W.-Y.; Che, C.-M. A High-Symmetry Coordination Cage from 38- or 62-Component Self-Assembly. *J. Am. Chem. Soc.* **2012**, *134*, 8042-8045.

(13) (a) Shivanyuk, A.; Rebek, J. Social Isomers in Encapsulation Complexes. *J. Am. Chem. Soc.* **2002**, *124*, 12074-12075. (b) Kobayashi, K.; Ishii, K.; Sakamoto, S.; Shirasaka, T.; Yamaguchi, K. Guest-Induced Assembly of Tetracarboxyl-Cavitand and Tetra(3-Pyridyl)-Cavitand into a Heterodimeric Capsule Via Hydrogen Bonds and CH−Halogen and/or CH−π Interaction: Control of the Orientation of the Encapsulated Guest. *J. Am. Chem. Soc.* **2003**, *125*, 10615-10624. (c) Shivanyuk, A.; Rebek, J., Isomeric Constellations of Encapsulation Complexes Store Information on the Nanometer Scale. Angew. Chem. Int. Ed. **2003**, *42*, 684-686. (d) Yamanaka, M.; Shivanyuk, A.; Rebek, J. Stereochemistry in Self-Assembled Encapsulation Complexes: Constellational Isomerism. *Proc. Natl. Acad. Sci. U.S.A.* **2004**, *101*, 2669-2672. (e) Ajami, D.; Theodorakopoulos, G.; Petsalakis, I. D.; Rebek Jr., J. Social Isomers of Picolines in a Small Space. *Chem. Eur. J.* **2013**, *19*, 17092-17096.

(14) (a) Abourahma, H.; Moulton, B.; Kravtsov, V.; Zaworotko, M. J. Supramolecular Isomerism in Coordination Compounds: Nanoscale Molecular Hexagons and Chains. *J. Am. Chem. Soc.* **2002**, *124*, 9990-9991. (b) du Plessis, M.; Barbour, L. J. Supramolecular Isomerism and Solvatomorphism in a Novel Coordination Compound. *Dalton. Trans.* **2012**, *41*, 3895-3898.

(15) (a) Timmerman, P.; Verboom, W.; van Veggel, F. C. J. M.; van Duynhoven, J. P. M.; Reinhoudt, D. N. A Novel Type of Stereoisomerism in Calix[4]Arene-Based Carceplexes. Angew. Chem. Int. Ed. Engl. **1994**, *33*, 2345-2348. (b) Tucci, F. C.; Rudkevich, D. M.; Rebek, J. Stereochemical Relationships between Encapsulated Molecules. *J. Am. Chem. Soc.* **1999**, *121*, 4928-4929. (c) Kobayashi, K.; Ishii, K.; Yamanaka, M. Orientational Isomerism and Binding Ability of Nonsymmetrical Guests Encapsulated in a Self-Assembling Heterodimeric Capsule. *Chem. Eur. J.* **2005**, *11*, 4725-4734.

(16) Tsuzuki, S.; Uchimaru, T.; Mikami, M.; Kitagawa, H.; Kobayashi, K. Mechanism of Orientational Isomerism of Unsymmetrical Guests in a Heterodimeric Capsule: Analysis by Ab Initio Molecular Orbital Calculations. *J. Phys. Chem B.* **2010**, *114*, 5335-5341.

(17) (a) Wild, A.; Winter, A.; Schlütter, F.; Schubert, U. S. Advances in the Field of Π-Conjugated 2,2′:6′,2″-Terpyridines. *Chem. Soc. Rev.* **2011**, *40*, 1459-1511. (b) Chakraborty, S.; Newkome, G. R. Terpyridine-Based Metallosupramolecular Constructs: Tailored Monomers to Precise 2d-Motifs and 3d-Metallocages. *Chem. Soc. Rev.* **2018**, *47*, 3991-4016. (c) Fu, J.-H.; Lee, Y.-H.; He, Y.-J.; Chan, Y.-T. Facile Self-Assembly of Metallo-Supramolecular Ring-in-Ring and Spiderweb Structures Using Multivalent Terpyridine Ligands. *Angew. Chem. Int. Ed.* **2015**, *54*, 6231-6235. (d) Wang, S.-Y.; Fu, J.-H.; Liang, Y.-P.; He, Y.-J.; Chen, Y.-S.; Chan, Y.-T. Metallo-Supramolecular Self-Assembly of a Multicomponent Ditrigon Based on Complementary Terpyridine Ligand Pairing. *J. Am. Chem. Soc.* **2016**, *138*, 3651-3654. (e) Zhang, Z.; Wang, H.; Wang, X.; Li, Y.; Song, B.; Bolarinwa, O.; Reese, R. A.; Zhang, T.; Wang, X.-Q.; Cai, J.; Xu, B.; Wang, M.; Liu, C.; Yang, H.-B.; Li, X. Supersnowflakes: Stepwise Self-Assembly and Dynamic Exchange of Rhombus Star-Shaped Supramolecules. *J. Am. Chem. Soc.* **2017**, *139*, 8174-8185.

(18) (a) Wang, H.; Li, Y.; Yu, H.; Song, B.; Lu, S.; Hao, X.-Q.; Zhang, Y.; Wang, M.; Hla, S.-W.; Li, X. Combining Synthesis and Self-Assembly in One Pot to Construct Complex 2d Metallo-Supramolecules Using Terpyridine and Pyrylium Salts. *J. Am. Chem. Soc.* **2019**, *141*, 13187-13195. (b) Zhang, Y.; Calupitan, J. P.; Rojas, T.; Tumbleson, R.; Erbland, G.; Kammerer, C.; Ajayi, T. M.; Wang, S.; Curtiss, L. A.; Ngo, A. T.; Ulloa, S. E.; Rapenne, G.; Hla, S. W. A Chiral Molecular Propeller Designed for Unidirectional Rotations on a Surface. *Nat. Commun.* **2019**, *10*, 3742-3751.

(19) (a) Feenstra, R. M. Scanning Tunneling Spectroscopy. *Surf. Sci.* **1994**, *299-300*, 965-979. (b) Xue, Y.; Datta, S.; Hong, S.; Reifenberger, R.; Henderson, J. I.; Kubiak, C. P. Negative Differential Resistance in the Scanning-Tunneling Spectroscopy of Organic Molecules. *Phys. Rev. B.* **1999**, *59*, R7852-R7855. (c) Venema, L. C.; Janssen, J. W.; Buitelaar, M. R.; Wildöer, J. W. G.; Lemay, S. G.; Kouwenhoven, L. P.; Dekker, C. Spatially Resolved Scanning Tunneling Spectroscopy on Single-Walled Carbon Nanotubes. *Phys. Rev. B.* **2000**, *62*, 5238-5244. (d) Li, Z.; Li, Y.; Zhao, Y.; Wang, H.; Zhang, Y.; Song, B.; Li, X.; Lu, S.; Hao, X.-Q.; Hla, S.-W.; Tu, Y.; Li, X. Synthesis of Metallopolymers and Direct Visualization of the Single Polymer Chain. *J. Am. Chem. Soc.* **2020**, *142*, 6196-6205.

(20) (a) Song, B.; Kandapal, S.; Gu, J.; Zhang, K.; Reese, A.; Ying, Y.; Wang, L.; Wang, H.; Li, Y.; Wang, M.; Lu, S.; Hao, X.-Q.; Li, X.; Xu, B.; Li, X. Self-Assembly of Polycyclic Supramolecules Using Linear Metal-Organic Ligands. *Nat. Commun.* **2018**, *9*, 4575-4584. (b) Wang, L.; Liu, R.; Gu, J.; Song, B.; Wang, H.; Jiang, X.; Zhang, K.; Han, X.; Hao, X.-Q.; Bai, S.; Wang, M.; Li, X.; Xu, B.; Li, X. Self-Assembly of Supramolecular Fractals from Generation 1 to 5. *J. Am. Chem. Soc.* **2018**, *140*, 14087-14096.

(21) (a) Vaidyanathan, Vaidyanathan G.; Nair, Balachandran U. Nucleobase Oxidation of DNA by (Terpyridyl)Chromium(III) Derivatives. *Eur. J. Inorg. Chem.* **2004**, *2004*, 1840-1846. (b) Zare, D.; Doistau, B.; Nozary, H.; Besnard, C.; Guénée, L.; Suffren, Y.; Pelé, A.-L.; Hauser, A.; Piguet, C. Cr^{III} as an Alternative to Ru^{II} in Metallo-Supramolecular Chemistry. *Dalton. Trans.* **2017**, *46*, 8992-9009.

(22) (a) Chow, H. S.; Constable, E. C.; Housecroft, C. E.; Kulicke, K. J.; Tao, Y. When Electron Exchange Is Chemical Exchange–Assignment of 1H NMR Spectra of Paramagnetic Cobalt(II)-2,2′:6′,2″-Terpyridine Complexes. *Dalton. Trans.* **2005**, *2*, 236-237. (b) Constable, E. C.; Harris, K.; Housecroft, C. E.; Neuburger, M.; Zampese, J. A. Turning {M(Tpy)2}N+ Embraces and CH···Π Interactions on and Off in Homoleptic Cobalt(II) and Cobalt(III) Bis(2,2′:6′,2″-Terpyridine) Complexes. *CrystEngComm.* **2010**, *12*, 2949-2961.

(23) (a) Field, M. J.; May, B. L.; Clements, P.; Tsanaktsidis, J.; Easton, C. J.; Lincoln, S. F. Intramolecular Complexation in Modified B-Cyclodextrins: A Preparative, Nuclear Magnetic Resonance and Ph Titration Study. *J. Chem. Soc., Perkin Trans.1* **2000**, *0*, 1251-1258. (b) Piguet, C. Five Thermodynamic Describers for Address-

ing Serendipity in the Self-Assembly of Polynuclear Complexes in Solution. *Chem. Commun.* **2010**, *46*, 6209-6231. (c) Ihara, T.; Ohura, H.; Shirahama, C.; Furuzono, T.; Shimada, H.; Matsuura, H.; Kitamura, Y. Metal Ion-Directed Dynamic Splicing of DNA through Global Conformational Change by Intramolecular Complexation. *Nat. Commun.* **2015**, *6*, 6640-6648.

(24) (a) Jennings, P.; Wright, P. Formation of a Molten Globule Intermediate Early in the Kinetic Folding Pathway of Apomyoglobin. *Science* **1993**, *262*, 892-896. (b) Dobson, C. M.; Šali, A.; Karplus, M. Protein Folding: A Perspective from Theory and Experiment. *Angew. Chem. Int. Ed.* **1998**, *37*, 868-893. (c) Zhang, M.; Abrams, C.; Wang, L.; Gizzi, A.; He, L.; Lin, R.; Chen, Y.; Loll, Patrick J.; Pascal, John M.; Zhang, J.-f. Structural Basis for Calmodulin as a Dynamic Calcium Sensor. *Structure*, **2012**, *20*, 911-923.

(25) (a) Newkome, G. R.; Wang, P.; Moorefield, C. N.; Cho, T. J.; Mohapatra, P. P.; Li, S.; Hwang, S.-H.; Lukoyanova, O.; Echegoyen, L.; Palagallo, J. A.; Iancu, V.; Hla, S.-W. Nanoassembly of a Fractal Polymer: A Molecular "Sierpinski Hexagonal Gasket". *Science* **2006**, *312*, 1782-1785. (b)Jiang, Z.; Li, Y.; Wang, M.; Liu, D.; Yuan, J.; Chen, M.; Wang, J.; Newkome, G. R.; Sun, W.; Li, X.; Wang, P. Constructing High-Generation Sierpiński Triangles by Molecular Puzzling. *Angew. Chem. Int. Ed.* **2017**, *56*, 11450-11455. (c) Wang, L.; Song, B.; Khalife, S.; Li, Y.; Ming, L.-J.; Bai, S.; Xu, Y.; Yu, H.; Wang, M.; Wang, H.; Li, X. Introducing Seven Transition Metal Ions into Terpyridine-Based Supramolecules: Self-Assembly and Dynamic Ligand Exchange Study. *J. Am. Chem. Soc.* **2020**, *142*, 1811-1821.

(26) (a) Hoaglund-Hyzer, C. S.; Counterman, A. E.; Clemmer, D. E. Anhydrous Protein Ions. *Chem. Rev.* **1999**, *99*, 3037-3080. (b) Kruve, A.; Caprice, K.; Lavendomme, R.; Wollschläger, J. M.; Schoder, S.; Schröder, H. V.; Nitschke, J. R.; Cougnon, F. B. L.; Schalley, C. A. Ion-Mobility Mass Spectrometry for the Rapid Determination of the Topology of Interlocked and Knotted Molecules. *Angew. Chem. Int. Ed.* **2019**, *58*, 11324-11328.

(27) (a) Li, X.; Chan, Y.-T.; Newkome, G. R.; Wesdemiotis, C. Gradient Tandem Mass Spectrometry Interfaced with Ion Mobility Separation for the Characterization of Supramolecular Architectures. *Anal. Chem.* **2011**, *83*, 1284-1290. (b) Song, B.; Zhang, Z.; Wang, K.; Hsu, C.-H.; Bolarinwa, O.; Wang, J.; Li, Y.; Yin, G.-Q.; Rivera, E.; Yang, H.-B.; Liu, C.; Xu, B.; Li, X. Direct Self-Assembly of a 2D and 3D Star of David. *Angew. Chem. Int. Ed.* **2017**, *56*, 5258-5262.

(28) (a) Ludlow III, J. M.; Guo, Z.; Schultz, A.; Sarkar, R.; Moorefield, C. N.; Wesdemiotis, C.; Newkome, G. R. Group 8 Metallomacrocycles – Synthesis, Characterization, and Stability. *Eur. J. Inorg. Chem.* **2015**, *2015*, 5662-5668. (b) Chakraborty, S.; Hong, W.; Endres, K. J.; Xie, T.-Z.; Wojtas, L.; Moorefield, C. N.; Wesdemiotis, C.; Newkome, G. R. Terpyridine-Based, Flexible Tripods: From a Highly Symmetric Nanosphere to Temperature-Dependent, Irreversible, 3D Isomeric Macromolecular Nanocages. *J. Am. Chem. Soc.* **2017**, 139, 3012-3020.

(29) (a) Ugurlu, O.; Haus, J.; Gunawan, A. A.; Thomas, M. G.; Maheshwari, S.; Tsapatsis, M.; Mkhoyan, K. A. Radiolysis to Knock-on Damage Transition in Zeolites under Electron Beam Irradiation. *Phys. Rev. B.* **2011**, *83*, 113408. (b) Susi, T.; Kotakoski, J.; Arenal, R.; Kurasch, S.; Jiang, H.; Skakalova, V.; Stephan, O.; Krasheninnikov, A. V.; Kauppinen, E. I.; Kaiser, U.; Meyer, J. C. Atomistic Description of Electron Beam Damage in Nitrogen-Doped Graphene and Single-Walled Carbon Nanotubes. *ACS Nano* **2012**, *6*, 8837-8846. (c) Egerton, R. F. Mechanisms of Radiation Damage in Beam-Sensitive Specimens, for Tem Accelerating Voltages between 10 and 300 Kv. *Microsc. Res. Tech.* **2012**, *75*, 1550-1556.

(30) (a) De Feyter, S.; De Schryver, F. C. Two-Dimensional Supramolecular Self-Assembly Probed by Scanning Tunneling Microscopy. *Chem. Soc. Rev.* **2003**, *32*, 139-150. (b) De Feyter, S.; De Schryver, F. C. Self-Assembly at the Liquid/Solid Interface: Stm Reveals. *J. Phys. Chem B.* **2005**, *109*, 4290-4302. (c) Stepanenko, V.; Würthner, F. Hierarchical Self-Assembly of Cyclic Dye Arrays into Two-Dimensional Honeycomb Nanonetworks. *Small* **2008**, *4*, 2158-2161.

(31) (a) Hirunsit, P. Electroreduction of Carbon Dioxide to Methane on Copper, Copper–Silver, and Copper–Gold Catalysts: A DFT Study. *J. Phys. Chem. C.* **2013**, *117*, 8262-8268. (b) Lin, C.-Y.; Zhang, L.; Zhao, Z.; Xia, Z. Design Principles for Covalent Organic Frameworks as Efficient Electrocatalysts in Clean Energy Conversion and Green Oxidizer Production. *Adv. Mater.* **2017**, 29, 1606635-1606642.

(32) King, R. B.; Silaghi-Dumitrescu, I.; Şovago, I. Kinetic Versus Thermodynamic Isomers of the Deltahedral Cobaltadicarbaboranes. *Inorg. Chem.* **2009**, *48*, 5088-5095.

TOC

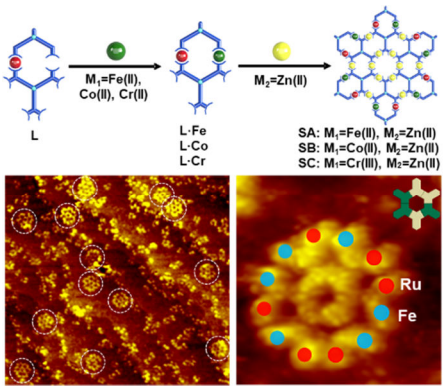
M1=Fe(II), Co(II), Cr(II)
M2=Zn(II)
L
L·Fe
L·Co
L·Cr
SA: M1=Fe(II), M2=Zn(II)
SB: M1=Co(II), M2=Zn(II)
SC: M1=Cr(III), M2=Zn(II)
Ru
Fe